

UC Riverside

UC Riverside Previously Published Works

Title

Novel Cranial Implants of Yttria-Stabilized Zirconia as Acoustic Windows for Ultrasonic Brain Therapy

Permalink

<https://escholarship.org/uc/item/6bv9m1h6>

Journal

Advanced Healthcare Materials, 6(21)

ISSN

2192-2640

Authors

Gutierrez, Mario I
Penilla, Elias H
Leija, Lorenzo
et al.

Publication Date

2017-11-01

DOI

10.1002/adhm.201700214

Peer reviewed

Novel Cranial Implants of Yttria-Stabilized Zirconia as Acoustic Windows for Ultrasonic Brain Therapy

Mario I. Gutierrez, Elias H. Penilla, Lorenzo Leija, Arturo Vera, Javier E. Garay,* and Guillermo Aguilar*

Therapeutic ultrasound can induce changes in tissues by means of thermal and nonthermal effects. It is proposed for treatment of some brain pathologies such as Alzheimer's, Parkinson's, Huntington's diseases, and cancer. However, cranium highly absorbs ultrasound reducing transmission efficiency. There are clinical applications of transcranial focused ultrasound and implantable ultrasound transducers proposed to address this problem. In this paper, biocompatible materials are proposed for replacing part of the cranium (cranial implants) based on low porosity polycrystalline 8 mol% yttria-stabilized-zirconia (8YSZ) ceramics as acoustic windows for brain therapy. In order to assess the viability of 8YSZ implants to effectively transmit ultrasound, various 8YSZ ceramics with different porosity are tested; their acoustic properties are measured; and the results are validated using finite element models simulating wave propagation to brain tissue through 8YSZ windows. The ultrasound attenuation is found to be linearly dependent on ceramics' porosity. Results for the nearly pore-free case indicate that 8YSZ is highly effective in transmitting ultrasound, with overall maximum transmission efficiency of $\approx 81\%$, compared to near total absorption of cranial bone. These results suggest that 8YSZ polycrystals could be suitable acoustic windows for ultrasound brain therapy at 1 MHz.

1. Introduction

Ultrasound therapies have been proposed for treatment of neurological disorders,^[1–4] such as Parkinson's disease,^[5] Huntington's disease,^[6] Alzheimer's disease,^[7–11] cancer,^[4,12,13] and others. Among the many benefits of ultrasound are that it can increase the uptake of low- and high-weight molecules into cells (sonoporation),^[14] can enhance gene transfer into cells (gene therapy),^[15] can dissolve blood clots during cerebral stroke (sonothrombolysis),^[16,17] can open the brain–blood barrier (BBB) to enhance drug and nanoparticles delivery,^[1,18–20] can enhance the levels of neurotrophic factors in brain that have a protective role of neurons,^[3] and can help with brain cancer therapy by sensitizing tumor cells to radiotherapy and chemotherapy,^[21,22] by opening the BBB, thus allowing drugs to reach the tumor,^[20,23] or by ablating the tumor with higher ultrasound intensities.^[4,12,13]

The greatest limitation to long-term use of ultrasound brain therapy is the cranium because it is a natural barrier that reflects about 50% of the energy back to the transducer due to mismatching of acoustic impedances of bone, soft tissues, and piezoelectric ceramics of ultrasound transducers,^[24] and of that 50% that is not reflected most is absorbed. For instance, at 1.8 MHz a 4 mm thick cranium absorbs nearly 90% of the ultrasound intensity that is not reflected.^[17] Absorption might be unavoidable, but the effect of reflection could be reduced by using adequate media for matching impedances between transducer and tissues.^[25] Although degassed water is usually preferred as a coupling medium to eliminate air gaps and for cooling the skin during high-intensity treatments,^[26] media capable of matching the impedances that can then increase energy transmission would be preferred.

In order to be able to use ultrasound for brain therapy, craniotomies have been used for single application therapies such as ablation,^[4] but they are not feasible for long repeated treatments that would require multiple cranial removals.^[27] Recently, an implantable transducer has been used to radiate directly into the brain;^[23] this approach has now been shown effective for opening the BBB in human trials and has improved drug delivery for cancer treatments. However, this technology still has some limitations for application. Because the entire implant consists of a biopackaged single frequency


Dr. M. I. Gutierrez
CONACYT—Instituto Nacional de Rehabilitación
Subdirección de Investigación Tecnológica
División de Investigación en Ingeniería Médica (DIIM)
Mexico City 14389, Mexico

Dr. E. H. Penilla
Mechanical and Aerospace Engineering
University of California San Diego
San Diego, CA 92161, USA

Dr. L. Leija, Dr. A. Vera
Department of Electrical Engineering, Bioelectronics
Centro de Investigación y de Estudios Avanzados del IPN
CINVESTAV-IPN
Mexico City 07360, Mexico

Dr. J. E. Garay
Mechanical and Aerospace Engineering
University of California San Diego
San Diego, CA 92161, USA
E-mail: jegaray@ucsd.edu

Dr. G. Aguilar
Department of Mechanical Engineering
University of California Riverside
Riverside, CA 92521, USA
E-mail: gaguilar@engr.ucr.edu

 The ORCID identification number(s) for the author(s) of this article can be found under <https://doi.org/10.1002/adhm.201700214>.

DOI: 10.1002/adhm.201700214

ultrasound transducer, the application range is limited, the transducer size is fixed to ≈ 10 mm diameter, and its invasiveness and cost limit the use of only single device implants. Our proposed paradigm has no limitation on frequencies and size, and it also has a reduced cost; it opens the possibility for multiple implants, ultimately for treatment of larger pathologies. In another way, transcranial magnetic resonance-guided focused ultrasound with transducer phase arrays, a technique that does not require craniotomy, has been effective under limited conditions. It has proved its feasibility in small animals with thin craniums;^[13,28] however, in humans, due to the human thicker cranium (thickness of 2–8 mm), it requires solving challenging technical issues as the larger absorption losses,^[27,29–31] and correcting phase aberration produced in the focal zone due to nonuniformities of cranium.^[2,32] Although these issues are somewhat solved,^[4,32] the time required for therapy planning and for the procedure plus the special conditions required for the application of ultrasound, i.e., shaving the patient head and monitoring the therapy with magnetic resonance imaging, makes this modality unfeasible for repeated treatments.^[23] Therefore, cost-effective solutions for long-term application of therapies are still needed.

Most bones of the skullcap (calvaria) consist of layers of compact bone (cortical bone) separated by diploë (cancellous bone) both being significant ultrasound attenuators. Ultrasound attenuation is caused by two major mechanisms: absorption and scattering.^[24] Absorption is the most effective attenuation mechanism and, although it is not fully understood so far, there are some hypotheses to explain it, mainly for liquids and homogeneous nonbiological solids.^[24,33,34] However, in solids and porous media (as bone), absorption is accompanied by other phenomena,^[24,35] namely, viscous friction effects produced by the motion of soft and solid media,^[24] scattering of ultrasound waves due to medium heterogeneity (internal mismatching of acoustic impedances in fluid-filled pores),^[35] and conversion of longitudinal waves to shear waves at the surface of scattering particles.^[35,36] These mechanisms are particularly important for cancellous bone composed of a larger proportion of soft and hard structures;^[24,35] however, attenuation in cortical bone is still large compared to that of soft tissues possibly due to the phenomena discussed above.^[24] Beam diffraction also has an important contribution in attenuation measurements,^[33] but its correction is easily applied during calculations.^[37]

In recent years, there has been an increasing interest in applying ceramic materials for biological purposes.^[38] This is in large part due to their biocompatibility^[39,40] and because they can provide high hardness^[41] and toughness,^[42] thus making them suitable for structural biological implants. Yttria-stabilized zirconia (YSZ) has been used to replace some damaged bones such as femoral heads in hip replacements,^[43] and zirconia crowns are often used in dental restoration.^[44] Recently, our group presented a pore-free transparent nanocrystalline 8 mol% yttria-stabilized zirconia (8YSZ) ceramic^[40,41,45] which can function as an optical/structural cranial implant and serve as an optical window to the brain (WttB), thus allowing the coupling of light directly into the cranial tissue for therapy.^[46] Along these lines, we surmised that 8YSZ with low porosity and nanoscale grain size could also be a low-attenuation media for ultrasound propagation.

Replacing cranium with 8YSZ implants could increase transmission of ultrasound because of their small acoustic attenuation affected by their nanoscale grain-size structure. In addition, ultrasound transmission is modified by the sample thickness (b),^[47] since this acts as a coupling layer between the transducer and the biological tissue. Then, the optimal energy transmission should be obtained with a thickness close to $b = \lambda/2$ (where λ is the wavelength in the ceramic sample). The effects of thermal transport losses, viscous friction, grain scattering, and mode conversion on bones and viscoelastic tissues^[24,33,35] do not have a significant contribution to absorption in our 8YSZ samples because of their small grain size (≈ 50 nm);^[48,49] however, forces among particles and beam diffraction still have a small but measurable contribution. We proposed the use of this 8YSZ formulation instead of others (3YSZ, 6YSZ, etc.) because it produces optically transparent ceramics^[46] that will permit us to propose an application of combined laser–ultrasound brain therapy. However, in situations where optical transparency is not required, 3YSZ, 6YSZ, and others can be used as an acoustic window to the brain, because the acoustic properties only vary slightly from those of 8YSZ, making 8YSZ a model system for investigating its applicability in each scenario. The acoustic window would also allow deeper penetration for treatment of interior brain pathologies that may not be accessible with light treatments alone and those cases were listed and discussed above.

In this paper, we present a finite element (FE) analysis of the implantable 8YSZ ceramics as a medium to transmit ultrasound more efficiently than the native cranial bone (Figure 1). We determined the acoustic properties of 8YSZ samples and, as such, the optimal conditions to efficiently transmit ultrasonic energy during continuous harmonic operation of a commercial ultrasound transducer. We also present, as an illustrative example, a measurement of ultrasound transmission through a sample of bovine cranium; a deeper analysis of bone samples is beyond the scope of this paper. The results suggest that 8YSZ can be used as a novel acoustic WttB with several

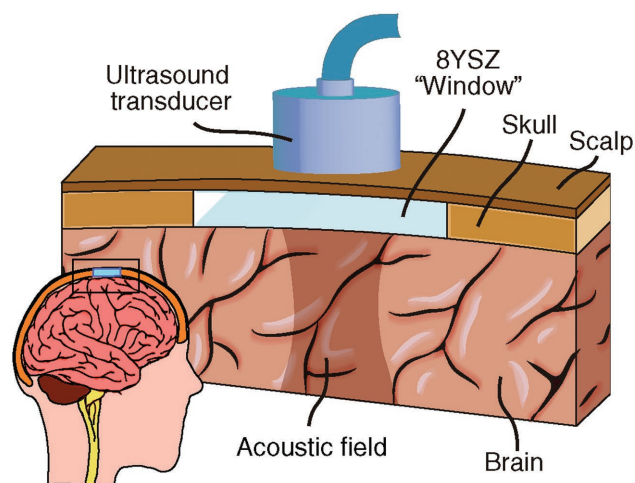


Figure 1. Schematic showing concept of 8YSZ ceramics as an “acoustic window to the brain.” Ultrasound transmission is significantly improved by using 8YSZ; ultrasound therapies in brain could vary.

possible ultrasound and combined laser–ultrasound applications, e.g., photoacoustic imaging.

2. Results

2.1. 8YSZ Samples Processing

As explained in the “Experimental Section,” 8YSZ samples were densified using current-activated pressure-assisted densification (CAPAD) at different temperatures. **Figure 2** shows the effect of CAPAD processing temperature on the relative density of 8YSZ ceramics. As expected, the relative density (ρ_r) increased with temperature ranging from $\approx 71\%$ at 850°C to 99% at 1200°C .

2.2. Acoustic Characterization

The acoustic parameters of different ceramic samples of 8YSZ were determined using the pulse–echo (PE) technique. We produced seven samples of 8YSZ with different thicknesses at 99% of average densification. The speed of sound of full dense 8YSZ samples was $7343.34 \pm 94.09 \text{ m s}^{-1}$. Other less dense samples were also made in order to determine the relationship between attenuation and density; samples of 3.6 mm thickness with densities of 95.8% , 87.6% , and 72.9% were produced. The transducer used for this work was made of barium titanate (BaTiO_3), which has a nominal acoustic impedance of 34.2 MRayls ,^[50,51] compared with the average impedance measured for 8YSZ samples $44.8 \pm 1.3 \text{ MRayls}$; these impedances are close enough to have a very small back reflection of the ultrasound energy. This is particularly important since the samples were attached to the transducer surface during the experiments, provoking a better energy transmission than if other media were placed between them; then, measured transmission will be mostly related to the attenuation than to the back reflection for impedance mismatching.

The impedance for different densities of 8YSZ samples is shown in **Figure 3A**; this graph is the result of the product of the measured speed of sound and the sample density. This

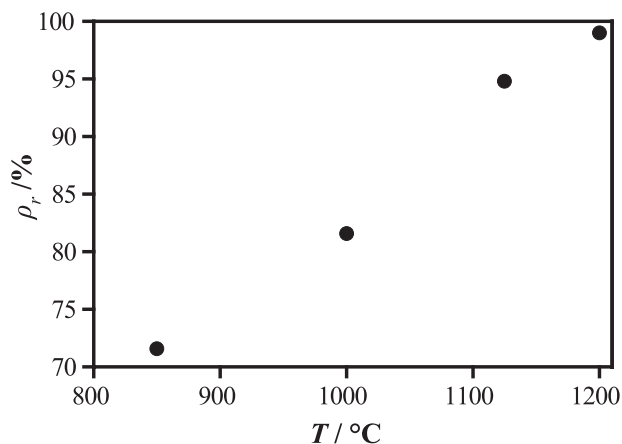


Figure 2. Effect of CAPAD processing temperature (T) on relative density (ρ_r) of 8YSZ samples.

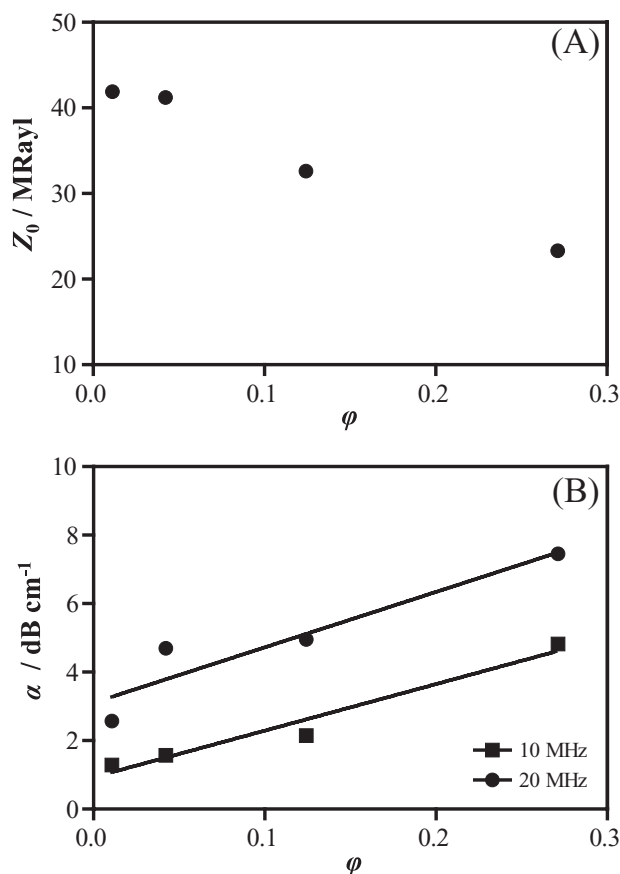


Figure 3. A) Acoustic impedance, Z_0 , and B) ultrasound attenuation, α , measured at 10 and 20 MHz, for different porosity, ϕ , of 8YSZ samples. Graphs show a linear tendency among measurements.

means that if the porosity changes, the speed of sound also changes; therefore, it is possible to adjust the impedance as required by following the tendency of graphs in **Figure 3**. However, lower impedance means more attenuation (**Figure 3B**). It could be possible to create an implant with different impedances along the thickness to gradually match the transducer and the tissues. The main results presented in this paper were obtained with fully dense samples, for which there was a certain energy reflection of 12.8% back to the transducer due to impedance mismatching. In a hypothetical case, in which the transducer should be coupled directly to the cranium or implant, i.e., after removal of the scalp, the impedance matching could have an important effect in transmission. The 12.8% of back reflection would be relatively small compared with that produced if the transducer were coupled directly to the cranium; if this backreflection is calculated using reported parameters for bone, tissues,^[31,52,53] and piezoelectric materials such as BaTiO_3 ,^[50,54] its value could be from 51% to 91% of the energy.

Attenuation was also an important factor to take into account. Measured acoustic attenuation of fully dense 8YSZ samples was $2.57 \pm 0.55 \text{ dB cm}^{-1}$ at 20 MHz (about $0.13 \text{ dB cm}^{-1} \text{ MHz}^{-1}$), which was low compared with that of cranial bone (28.08 dB cm^{-1} at 1.8 MHz or $15.60 \text{ dB cm}^{-1} \text{ MHz}^{-1}$).^[17] Hence, calculated attenuation for the fully dense samples at 1 MHz is 0.13 dB cm^{-1} (supposing a linear behavior

with frequency), which means 8YSZ ceramics do not significantly absorb the ultrasonic energy at this frequency. However, in 8YSZ ceramics, attenuation depends on sample porosity, as seen in Figure 3, from which it is clear that there is a linear relationship between these two parameters. This tendency could indicate that material porosity has an effect in 8YSZ ultrasound attenuation by means of an increase in scattering. Considering that the samples have the same grain size, bulk density would depend on how much “empty” space there is among 8YSZ grains. Thus, porosity increases ultrasound scattering and increases ultrasound attenuation. These assumptions are not applicable for other materials such as polymers, in which porosity is small but attenuation is large and depends on other material characteristics.

If attenuation is low for fully dense 8YSZ samples, ultrasound transmission will mainly depend on sample thickness. 8YSZ samples would work as acoustic coupling layers between the transducer and the brain. Based on this idea, the best energy transmission will occur when 8YSZ thickness is half of the ultrasound wavelength in the sample.^[17] This hypothesis was proven with the measurement of the acoustic field produced when samples were attached to the radiating surface of the ultrasound transducer.

2.3. Acoustic Transmission Analysis

The acoustic field was measured at 1 MHz using the 3D scanning system described in the “Experimental Section: Acoustic Field measurements.” Measurements were made on a 1 MHz commercial transducer, and the samples were attached to the radiating surface. Acoustic fields were postprocessed in order to quantify the energy transmitted. A bovine cranium bone was used as a model system in order to roughly compare our results with 8YSZ samples. A comprehensive analysis of the properties of different thickness of cranium was not carried out since it is broadly described in literature.^[17,31,53] Instead, a sample of bovine cranium bone was used as an illustrative example of how the high attenuation reduced dramatically the energy transmitted for thicknesses from 6 to 8 mm. Acoustic properties of human cranium are very close to those of bovine.^[53] Actually, human cranium properties could be in a wide range of values that make cranial bone a difficult medium to study.^[31,55]

The profiles measured along the diameter at 2 mm from the radiating surface (YSZ sample, bone, or transducer) are shown in Figure 4. Although lateral lobes (radiation coming from the noncovered part of the transducer) are not of interest for this work, they are shown in Figure 4 in order to compare the levels of pressure among measurements with different samples. Bone shows the most intense reduction in amplitude due to its large absorption.^[17] Bone transmitted 2.8% of the energy when the thickness was 6 mm, and 1.2% of the energy at 8 mm. In fact, a large portion of the energy (more than 97%) remained in the sample and was converted into heat. The 8YSZ sample with 3.6 mm of thickness ($\approx \lambda/2$) permits an excellent transmission to the water of 80.8% of the energy, but it modifies the pressure distribution; notice that the peaks in the profiles measured with no sample and with 3.6 mm sample are not in the same position. This indicates that the radiation coming from the 8YSZ is

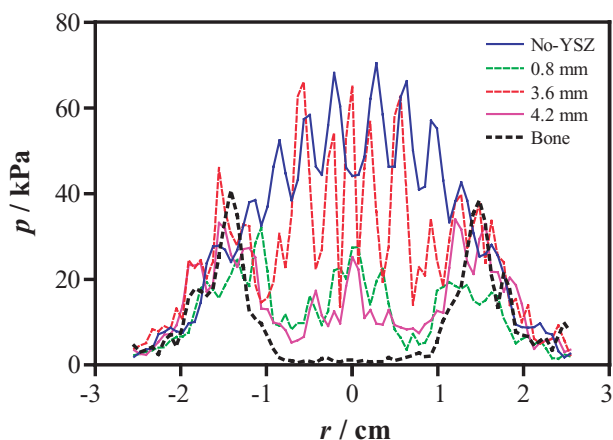


Figure 4. Acoustic pressure (p) at 2 mm from the radiating surface when 8YSZ samples and bone were attached to the transducer. Notice that the 8YSZ samples (1.96 cm diameter) did not cover the entire surface of the transducer (4.2 cm diameter). Lateral lobes are not important for this work, but are shown to illustrate that the radiation among the different graphs is comparable. Graphs for three different sample thicknesses are shown. Two other thicknesses were omitted since results were similar to those of 0.8 and 4.2 mm.

the result of the own 8YSZ resonant vibration that apparently is independent of the transducer radiating profile. This result has implications for future works since it should be considered that the acoustic field distribution after the sample would only depend on the sample vibration; thus producing a profile dependent on its own geometry. Therefore, it may not be necessary to determine and account the vibration profile of the piezoelectric transducer for modeling 8YSZ vibration. This nondependence was observed during this work but was not fully analyzed.

Multiple simulations for each thickness of the 8YSZs attached on the transducer surface were run in order to determine the best energy transmission in relation to the thickness (more details in the “Experimental Section: Postprocessing Acoustic Field”). These results are shown in Figure 5A. The efficiency of electrical-to-mechanical energy conversion was set to 61% as measured for this transducer at 1 W (data not shown). Because the 8YSZ did not cover the entire transducer surface, another set of simulations with an ideal reflector ($Z \approx 0$) for the same different thicknesses used in 8YSZ simulations was carried out. This ideal reflector did not allow ultrasound to go through. These simulations were designed in order to determine how much radiation coming from the part not covered by the 8YSZ (rim radiation) reached the region of interest. With this information, it was possible to determine a volume, which should be large enough to get as much data as possible, required for postprocessing immediately after the sample. It was also determined that the radiation coming from the rim was not important, since it was less than 1.5 kPa, which is lower than 10% of the smaller average pressure in the graph showed in Figure 5A. Moreover, Figure 5B shows another two set of simulations when the transducer is radiating through 5 mm thick scalp^[56] when either the cranium or the 8YSZ is placed. 8YSZ still transmits better than bone even if the ceramic is not in contact with the transducer, thus repeating a resonance at $\lambda/2$ (3.6 mm thickness).

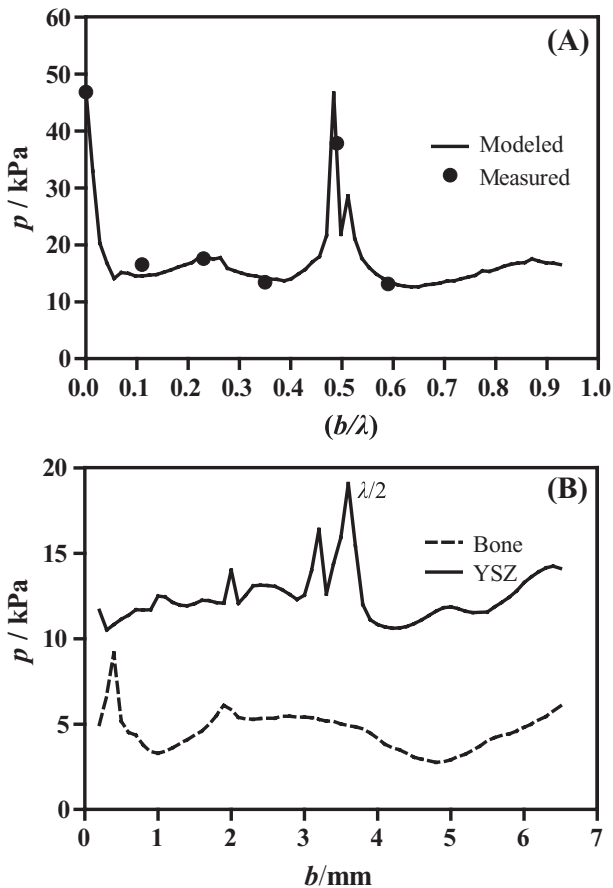


Figure 5. A) Acoustic pressure (p) averaged after 8YSZ samples versus normalized thickness. Thickness (b) was normalized with the sample wavelength (λ). Large dots (●) represent experimental data points with the 8YSZ samples of different thickness, and the continue line represents the modeling results. B) Acoustic pressure (p) averaged after 8YSZ samples (continue line) and bone (dashed line) versus thickness when the transducer was radiating through a 5 mm scalp. Thickness was not normalized as the graph in part (A), because both materials (8YSZ and bone) have different wavelengths. However, the maximum transmission was still in $\lambda/2$, as indicated. In both graphs, acoustic pressure was averaged into a cylinder of $r = 8$ mm and 1 cm of depth.

Representative measured and modeled acoustic fields are shown in **Figure 6** for different thicknesses of 8YSZ samples. Modeling parameters are detailed in the “Experimental Section: Modeling Conditions.” For these figures, the acoustic field of uncovered region of the radiating surface was omitted; therefore, only the field that goes through the sample can be seen. The fields are similar but with slight variations in the acoustic profile. Although the distribution of models and measurements is not identical, they have certain resemblance between the fields of the same sample.

3. Discussion

The results of the previous section show that ultrasound can be transmitted more efficiently through 8YSZ samples than through cranial bone. We chose 8YSZ formulation because it

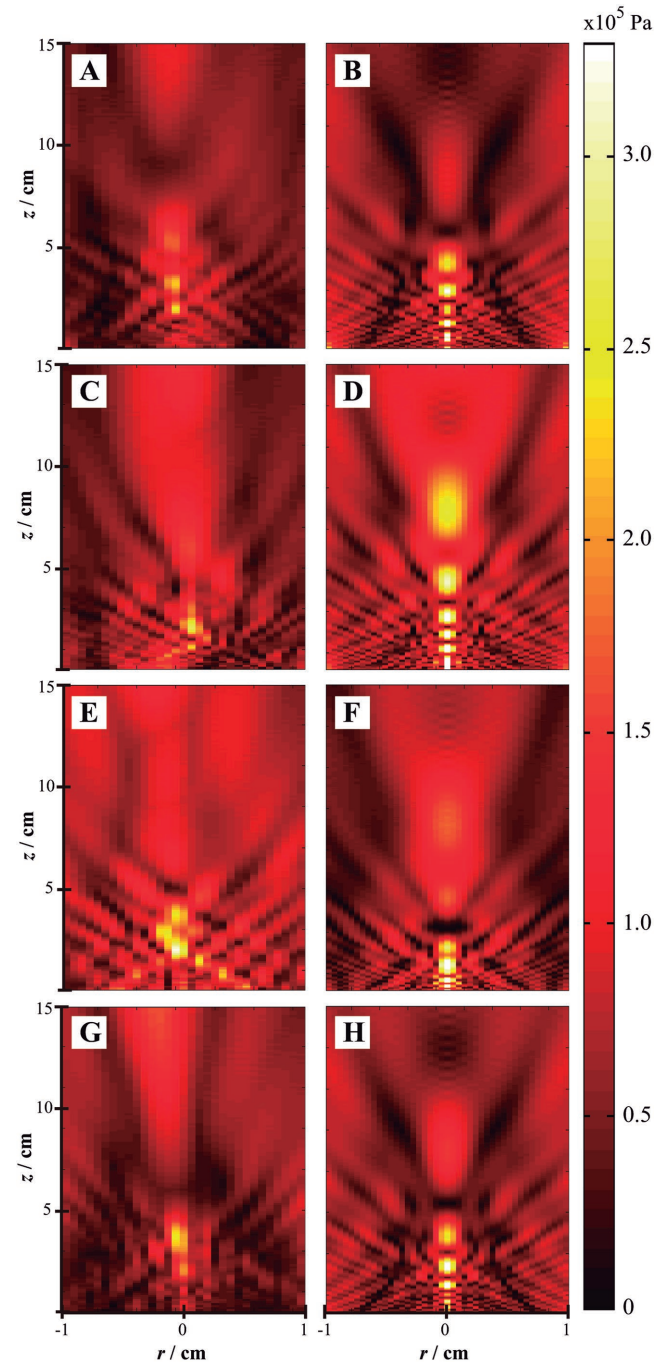


Figure 6. Acoustic field in water using 8YSZ samples of different thickness (b). Left column: measurements; right column: models. A,B) 8YSZ thickness is 0.8 mm; C,D) 1.6 mm; E,F) 3.6 mm; and G,H) 4.2 mm.

can be optically transparent as already presented by our group in a previous publication.^[46] This transparency plus the capability of transmitting ultrasound will permit us to propose an optoacoustic WttB to be used in combined laser–ultrasound brain therapy or simply as an acoustic WttB when photonic therapy is not required. Attenuation and impedance mismatching are the main phenomena that reduce ultrasound transmission through bone. Attenuation could be addressed by using our

proposed ceramic implants. Our measurements were correctly represented by the models, as can be seen in Figures 3–6. We can notice that there is a clear dependence between transmission and sample thickness. Moreover, ultrasound attenuation depends on sample bulk density.

Acoustic impedance and attenuation were measured as a function of porosity (Figure 3). Changes in impedance were mainly due to changes in the speed of sound, which depends on the elastic properties and the density of the sample. This finding will be useful for future works because it would allow designing the material based on the tissue parameters, thus providing an efficient transmission, in terms of acoustic impedance, but with an increase in attenuation. Attenuation plays an important role here, and it changes inversely to density; then, more attenuation means less energy in the tissue. As expected, attenuation changed proportionally with the relative density because of the presence of more pores in the material. Considering that the sample volume and the grain size were kept constant, the bulk density would depend on material porosity. Even if the grain size were small enough to neglect absorption by grain scattering, an increase in porosity may change this parameter. The linear relationship between bulk density and attenuation in Figure 3B implies that porosity increased ultrasound attenuation in our 8YSZ samples. This could be caused by increasing ultrasound scattering in the sample, even for small grain sizes.

From the overall results, we notice that the 8YSZ samples did not have 100% of ultrasound transmission. Energy could be lost due to diverse factors as ultrasound absorption at different layers, ultrasound diffraction, beam dispersion, impedance mismatching provoking repetitive back reflections, and attenuation by grain scattering. Our FE model includes, by default, most of them, except losses by ultrasound diffraction and attenuation by grain scattering. The diffraction effect was not fully accounted for because we are using an ideal radiator (piston) with a different diffraction pattern than our experimental transducer;^[57] the grain-scattering effect for these samples should be small because the grain size is notably smaller (≈ 50 nm) than the ultrasound wavelength (≈ 7.2 mm).^[48,49] The causes of losses of transmission explained here are true for ceramics, but not for polymers, which have large acoustic attenuations mainly because of material composition, not porosity or grain scattering. The use of polymers as acoustic WtB would be not adequate because of their large intrinsic attenuations.

Moreover, having a layer of glue between the transducer and the 8YSZ samples did not change the energy transmission and permitted the separation of the effects of vibration and pressure in the models. For instance, if the 8YSZ were perfectly attached to the transducer, the vibration of the latter would be significantly modified thus creating a whole new ultrasound transducer. Because of this uncoupling effect, the sample vibrated on its own resonant mode, radiating ultrasound by itself (resonator) and also transmitting the ultrasound coming from the transducer (coupling media); both effects were considered in the FE models by interconnecting structural mechanics (plus piezoelectric effect) and acoustics. This behavior can be seen in the peak distribution of the 3.6 mm sample in Figure 4. This peak distribution does not match with the peak distribution of radiation with no sample, which implies that the sample is not

just transmitting ultrasound but is also resonating and then creating its own field, thus increasing the overall transmission efficiency. This resonance can be adjusted by changing the shape (thickness and diameter) and the mechanical properties of the sample (density, Young's module, and Poisson's ratio), by adjusting the processing conditions in CAPAD.

Also from Figure 4, the improvement of the transmitted energy of the 8YSZ sample of 3.6 mm thickness is obvious. Other analyzed samples showed lower transmission, which indicates dependence on the sample thickness, as other acoustic properties did not change (Figure 5A).^[58,59] Assuming a coupling layer of infinite radius and finite thickness, the most efficient energy transmission for air-backed narrowband transducers can be obtained when the layer has a thickness of $\lambda/2$.^[25,58] The results demonstrate that the best transmission occurred when the thickness is close to $\lambda/2$, because the optimal transmission of energy with a disk of finite radius will be a little larger than $\lambda/2$. Apparently, with this experimental setup, 8YSZ ceramics work as transducer-coupling layer for acoustic matching in two ways, improving transmission by impedance matching and keeping efficiency by self-resonating. Result simulations in Figure 5B, with the transducer radiating through the scalp, show that 8YSZ still permits a better ultrasound transmission than cranial bone; it can also be seen as increased transmission in 3.6 mm thick 8YSZ, which corresponds to $\lambda/2$ thickness. Simulations with the bone instead of the 8YSZ show that the overall transmission through bone is importantly reduced by absorption losses. Actually, these simulations did not include the effect of diploë scattering,^[55] which has shown to be an important source of ultrasound attenuation.

There is also an effect when the thickness is close to $\lambda/4$, which is useful for wideband applications.^[25] Figure 5A shows an increase in the acoustic pressure at $\lambda/4$ thickness that could be useful for nondestructive testing (NDT), also observed in Figure 5B; coupling layers of $\lambda/4$ are commonly used to increase the bandwidth of the transducers.^[59] Applications of pulse–echo in brain could be plausible, as diagnostic imaging and NDT. This would be advantageous because the bioimplantable ceramic would serve as a treatment and assessment window, during repeated treatment scenarios. Transducers specially designed for reception (and transception) can be used for detecting ultrasound produced by other sources such as lasers (photoacoustics) or optical cavitation (shockwave formation with laser); 8YSZ implants can help transmit both ultrasound and laser light to the brain.^[46] Other applications may arise if the shape of the implant is modified to get acoustic focalization when using a concave 8YSZ implant. However, this research is outside of the scope of this paper as we are not proposing this paradigm for ablation therapies; its use in those scenarios may also be a viable alternative to currently existing and implemented technologies.

As an illustrative view, the measured and modeled acoustic fields of the transducer with different 8YSZ samples attached on the radiating surface are shown in Figure 6. In this figure, the lateral lobes coming from the uncovered transducer surface were omitted. It can be observed that the radiation through the samples was adequately modeled with the FE analysis, because the pressure distribution along the propagation axis

was similarly distributed. The averaged pressures used for Figure 5A were extracted from these data. The best transmission was obtained with the 8YSZ sample of 3.6 mm thickness. The observed diffraction in the acoustic fields is representative from planar transducers,^[57] and it is composed by local maxima and minima of pressure produced by constructive and destructive interferences in the near-field zone (Fresnel zone). The purpose of this work is to provide nonfocalized low intensity ultrasound brain therapy; hence, this diffraction pattern does not represent a problem for this intended application.

The models presented in this paper were based on the experimental setup proposed to characterize the ultrasound transmission of the samples. These provided us an insight into how these ceramics work with acoustic energy. However, the conclusions presented in this paper are limited by the assumptions made to produce those models and the simplifications used for the experimental setup. For instance, the use of glue to attach the samples to the transducer could be a source of error that should be accounted for future experiments; however, in our results the effect of the glue was negligible. When including the scalp in the system, either in the experiments or in the models, an effect of stationary waves will be present. This effect is related to the materials' speed of sound and density, and it resembles the effect of resonance observed in the samples at $\lambda/2$. Although in the 8YSZ samples this effect is desirable, in the scalp it is not. Stationary waves will be producing important heating in the scalp, which would provoke in the patient discomfort or even injuries. This effect should be accounted in future work if the transducer is planned to be stationary during treatments.

4. Conclusion

The results presented here demonstrate the viability of using 8YSZ ceramics to efficiently transmit ultrasound. A linear relationship between ultrasound attenuation and material bulk density was found, which could present porosity as another variable that modifies ultrasound absorption in ceramic samples. This variable is additional to the already studied absorption by grain scattering and mode conversion in microstructures.^[48] With the full dense samples, we obtained 80.8% of ultrasound transmission through an 8YSZ implant of 3.6 mm, in contrast to almost 10% of reported ultrasound transmission through cranial bone at the same thickness.^[17]

Our group previously proposed the use of these materials as cranial implants in order to create optical WttB for brain therapy; the applicability of these implants to other kind of energy, the ultrasound, was extended in this paper. After this work, we can propose combined optoacoustic modalities for treatment or diagnosis which would allow having a wide variety of possible applications. For instance, using concave ceramics would permit us to focalize the waves in a specific region of the brain. However, research should continue to fully characterize the materials in the environment where they should be implanted to know how their properties could affect their behavior with the different energies to be used during the treatments. More research about medical applications of both laser and ultrasound in brain should be carried out.

5. Experimental Section

YSZ Sample Preparation: For this work, commercial (Tosoh Corporation, Tokyo, Japan) nanocrystalline 8YSZ powder (TZ-8Y) with a reported grain size of 50 nm was densified using CAPAD. Prior to densification the as-received powder was low-energy ballmilled in ultra-high purity H₂O at 100 rpm using 5 mol% YSZ (5YSZ) spherical milling media (also from Tosoh Corporation). The milling medium's diameter was 5 mm in all cases. The powder mass to milling media and UHP H₂O mass ratio was 1:20:20 so that 10 g of powder was milled with 200 g of media within 200 g of UHP H₂O. The total milling time was 6 h. After milling the powder was sieved in order to separate out the milling media. The 8YSZ and UHP H₂O slurry was centrifuged at 3400 rpm for 10 min to remove the water. The centrifuged powder was then dried in a vacuum oven at 70 °C for 24 h. After drying, the powder was crushed in a mortar and sieved using a 325 mesh, and it was stored dry until CAPAD processing.

Current-activated pressure-assisted densification was implemented to produce high-density, fine-grained undoped 8YSZ polycrystals. For this work, a two-step mechanical loading with simultaneous heating route similar to the one used in previous work was implemented.^[60] In brief, 19 mm graphite tooling was used for densification within a custom CAPAD apparatus.^[61] In order to produce samples with variance in thickness, the sample mass was varied from 1.5000 ± 0.0001 to 7.5000 ± 0.0001 g. In order to minimize thermal gradients in the samples as the thickness varied, this graphite tooling was insulated during CAPAD processing with a graphite felt jacket of ≈ 1 cm thickness.

Following densification and sample extraction from the graphite tooling, the 8YSZ polycrystals were mounted with crystal bond adhesive to a ground and hardened tool steel backing plate, and they were mechanically polished to their final thicknesses (0.8, 1.6, 2.5, 3.0, 3.6, and 4.2 mm) using polycrystalline diamond particles suspended in polyethylene glycol. The final diamond grit size was 0.05 μ m. The bulk density of the polished samples was measured using the Archimedes method and porosity (ϕ) was determined using

$$\phi = 1 - \rho_r \quad (1)$$

where ρ_r is relative density calculated with the measured density divided by 8YSZ theoretical density.

Bovine Cranial Bone Sample: A bone sample of bovine cranium was used for a comparison of this main results. The sample was prepared from the cranial frontal bone of an adult male bovine (crossbred of cebuine and brown swiss). Bone was collected from a slaughterhouse 6 h after the animal was killed and it was immersed in 0.9% saline solution immediately after its collection (9.0 g of NaCl per liter of water). The sample was cut to have a round shape of 1.95 cm of diameter (same size of 8YSZ samples), but was avoided cutting other surfaces to keep bone layers of cranium intact (compact bone and diploë); a region without important reliefs of corneal process was preferred. **Figure 7** shows the cranial frontal bone before preparation (parts (A) and (B)) and the final sample (parts (C)–(E)). The final thickness varied from 6 to 8 mm, so the results were analyzed accordingly to this variation.

Acoustic Characterization: Two main acoustic parameters of 8YSZ samples were measured: speed of sound and ultrasound attenuation. Speed of sound (SOS) of samples was determined with PE using a 20 MHz contact ultrasound transducer (V116-RM, Olympus Corp., USA) as shown in **Figure 8**. For these measurements, a homemade pulser was designed on the basis of ref. [62]; the echo received was amplified by a wideband amplifier (SR445, SRS, USA) before being registered by the oscilloscope (TDS3014B, Tektronix, USA). The samples were manufactured with 1.96 cm of diameter with different thicknesses ranging from 0.8 to 4.2 mm. A 20 MHz transducer was preferred in order to have at least four cycles traveling into the thinnest sample (0.8 mm); this transducer, driven with a short excitation spike (<25 ns), allowed obtaining multireflected separated echoes. The SOS was calculated with the measured sample thickness and the time between repeated echoes using the formula $c = 2b/t$, where b is the sample thickness and

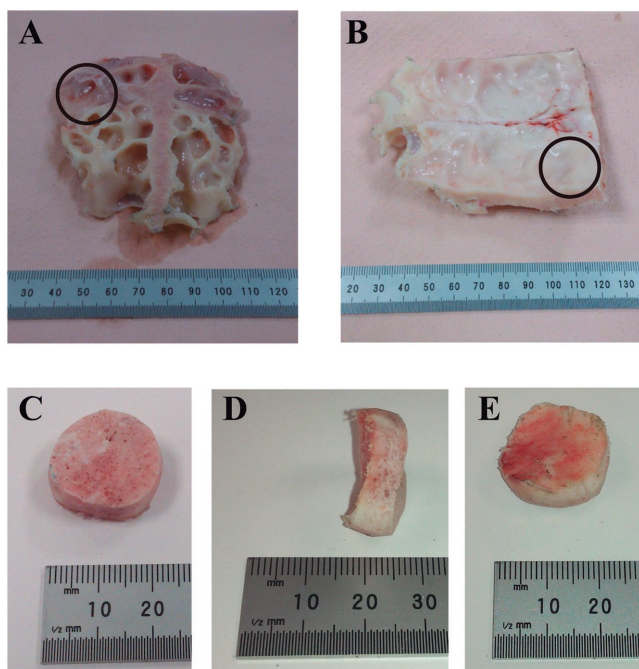


Figure 7. Sample of cranial bone of an adult male bovine. A,B) Top and bottom views of cranial frontal bone with the cornual process; circles indicate the region where the sample was extracted. C–E) Different views of the bone sample obtained from the cranial frontal bone with a circular shape of 1.95 cm of diameter and 6–8 mm of thickness.

t is the time difference between echoes; this time difference was found by autocorrelation. Characteristic acoustic impedance (Z_0) of 8YSZ samples was determined by the product of SOS and the material bulk density, $Z_0 = \rho c$.

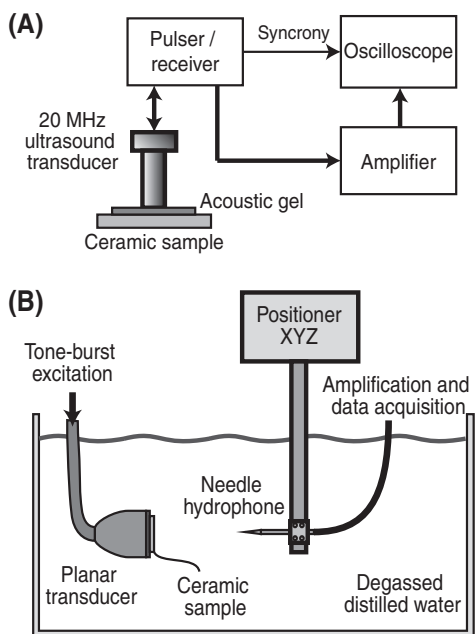


Figure 8. Setup for acoustic characterization. A) Pulse–echo setup using a contact transducer. B) Setup to measure the acoustic field in water with needle hydrophone. C) Photograph of commercial ultrasound transducer with an 8YSZ sample attached to the radiating surface; the sample did not cover the entire surface.

The acoustic attenuation (α) of the thicker samples (4.2, 3.6, and 2.5 mm) was determined with pulse–echo; thicker samples were used to get separated echoes, and it was assumed that the rest of the samples had a similar behavior. In order to have separated echoes, two transducers of 10 MHz (V312-SU, Olympus Corp., USA) and 20 MHz (V317-SU, Olympus Corp., USA) were placed on the sample; air was kept after the sample to increase ultrasound reflection. Acoustic gel (Aquasonic 100, Parker laboratories, Inc., USA) was required as the contact medium at the interface of transducer/sample; during the measurements, the transducer and the sample were not in contact, but a regular space was kept between them. Repeated echoes produced by the interface sample/air were taken; the very first echo was discarded for attenuation calculation. Four repeated echoes were acquired for each sample, so three measurements could be possible. Attenuation was determined with the amplitude spectra of received echoes with the next equation

$$\alpha(f) = \frac{1}{2L} \left(\ln(R) + \ln \left(\frac{A_{n_1}(f)}{A_{n_2}(f)} \right) \right) \quad (2)$$

where L is the sample thickness, which is traveled twice by the echoes, A_{n_1} and A_{n_2} are the amplitude spectra of pulse 1 and 2, respectively; f is the frequency of amplitude spectra; and R is the reflection coefficient from the sample to acoustic gel in terms of acoustic impedances of gel Z_G and sample Z_0 given by

$$R = \left| \frac{Z_G - Z_0}{Z_G + Z_0} \right| \quad (3)$$

Acoustic Field Measurements: The commercial transducer of 1 MHz used for the acoustic field measurements is composed by a piezoelectric disk of BaTiO₃ and a frontal protective layer of glass (model 7310, Mettler Electronics Corp., USA);^[57,63] this front layer did not affect significantly the transducer response because of its small thickness which was determined by PE using the buffer rod technique with a 20 MHz ultrasound transducer (V317-SU, Olympus Corp., USA).^[64] Transducer radiating surface is 4.2 cm of diameter, with an effective radiating area (A_{ER}) of 8.19 cm². The 8YSZ samples were attached with silicone glue (Mil'U, Cromher, Mexico) to the transducer radiating surface; acoustic properties of this glue are close to those of scalp (see Table 1), so this would allow making some comparisons with a model including the scalp. However, samples did not cover the entire radiating surface, which should be considered for determining the transmitted acoustic field. The protective layer and sample/transducer dimensions were included in the FE analysis in order to quantify their effect.

Ultrasound was measured after the sample while it was coupled to the piezoelectric ceramic resonator. The transducer with the sample was immersed in distilled degassed water at 20 °C, and the acoustic field was measured at each spatial point. The transducer was driven using a radiofrequency (RF) wave generator (Array 3400, China) with 25 sine cycles tone burst of 20 Vp–p, at 1 ms repetition rate. Using tone burst instead of a single pulse or continued sine wave allowed simulating a nearly continuous emission, but avoiding errors due to wave reflections at the tank walls by permitting the system to dissipate the energy before the next measurement. In order to get the most energy transmission, the frequency of the RF generator was adjusted accordingly to the thickness extensional (TE) vibration mode observed in the electric impedance of the transducer with the sample attached measured with an impedance analyzer (Agilent 4294A, USA); this adjustment was less than 3% of the frequency without sample (998 kHz).



Table 1. Properties of the materials used in the FE models.^[50,51,70,71]

Property	8YSZ	BaTiO ₃ ^[50]	Glass ^[71]	Silicone glue ^[72]	Water ^[70]	Scalp ^[73–75]	Cortical bone ^[17,31,76,77]	Diploë ^[55]
Young's modulus [GPa]	274.1 ^{a)}	–	70	0.05	–	0.05	20.7	–
Poisson's ratio	0.23	–	0.22	0.49	–	0.49	0.15	–
Speed of sound [m s ⁻¹]	7343 ^{b)}	5850	3962	1485 ^{b)}	1497	1600	3489	2500
Density [kg m ⁻³]	5893 ^{b)}	5620	2500	1500 ^{b)}	997	1100	2543	1740
Isotropic loss factor	0.01	0.01	0.01	0.01	–	0.01	0.01	–
Acoustic attenuation [dB cm ⁻¹ MHz ⁻¹]	0.13 ^{b)}	0.02	0.02	–	0	0.5	15.60	13.03
Elasticity matrix [GPa] (c_{ij}^E , ordering: $ij = 11, 12, 13, 33, 44, 66$) ^{c)}	–	150.4, 65.6, 65.9, 145.5, 43.8, 42.4	–	–	–	–	–	–
Piezoelectric matrix [C m ⁻²] (e_{ij} , ordering: $ij = 31, 33, 15$) ^{c)}	–	–4.32, 15.6, 11.4	–	–	–	–	–	–
Relative permittivity (ϵ_{ij}^S , ordering: $i = 1, 3$) ^{c)}	–	1115.1, 1251.3	–	–	–	–	–	–

^{a)}Calculated using basic relations; ^{b)}Measured by our group; ^{c)}Obtained from COMSOL Multiphysics material library, which are close to those reported by Berlincourt.^[50,51]

The acoustic pressure was measured using a wideband needle hydrophone (PZT244-0400, Onda Corp., USA) with an effective aperture of 0.4 mm and a sensitivity of -260 dB, referred to as $1 \text{ V } \mu\text{Pa}^{-1}$ at 1 MHz. The hydrophone was mounted on a 3D scanning automated system (Scan 340, Onda Corp., USA) in order to measure the pressure at each spatial point. Several measurements were carried out. A first sequence of measurements was made for centering the hydrophone with the emission. The center of the acoustic field was chosen in accordance with an equally distributed radiating energy of the emission at 2 mm from the 8YSZ sample. This center location was confirmed at 150 mm with a deviation smaller than 2 mm in the x -axis. After centering the emission, a xz pressure plane starting at 2 mm from the sample and finishing after 15 cm was acquired for each sample. The resolution of each step in the x -direction was 0.7 mm (about half of a wavelength in water) and 1.0 mm in the z -direction limited by the measurement system.

Modeling Conditions: Models were obtained with the FE method in the harmonic stable-state operation working in the TE vibration mode. Based on the characteristics of the transducer radiation and the cylindrical shape of 8YSZ samples, the model was considered axisymmetric and the geometry was simplified to the one shown in **Figure 9**. Two analyses were developed simultaneously in order to model the field transmitted through the ceramic: a piezoelectric part which involved the transducer (and its protective layer) together with the 8YSZ sample, and an acoustic pressure model which considered all the layers that transmit ultrasound, including the transducer. In order to simplify the solution, the transducer was considered as a piston in which only z -displacements were permitted at the rim. The transducer is composed of a piezoelectric domain of BaTiO₃ with 2.51 mm thickness and 2.1 cm radius, and a glass protective layer of 160 μm which covered the radiating surface. 8YSZ samples were attached with silicone glue which created an uncoupling effect between the sample and the transducer included in the model. Therefore, between the glass and the 8YSZ sample, a thin layer of glue (100 μm) was included as shown in the zoom of **Figure 9**. Simulations were solved in the frequency domain, for different thicknesses of the sample, which varied from 0.1 to 9.0 mm in steps of 0.1 mm.

Moreover, another set of simulations were carried out to analyze the effect of 5 mm thick scalp.^[56] This tissue was included instead of the glue layer. **Figure 9** is still valid for this model, but with a scalp layer of 5 mm instead of the glue layer. The transducer was radiating through both the scalp and the sample. Two conditions were analyzed for the sample: the use of 8YSZ ceramic as previously explained, and the use of a cranial bone. Cranial bone was considered to be composed by two layers of cortical bone and an intermediate layer of diploë; cortical bone layers were set to represent 30% of the total thickness each, while

the other, diploë layer, was set to 30% of total thickness. Also, these simulations were solved in the frequency domain and for different thicknesses of the samples, as the previously explained simulation.

The equations of harmonic vibration of piezoelectric disks have been fully described in literature.^[65–67] It can be started from the constitutive equations given by

$$\sigma = c^E \epsilon - e^T E \quad (4)$$

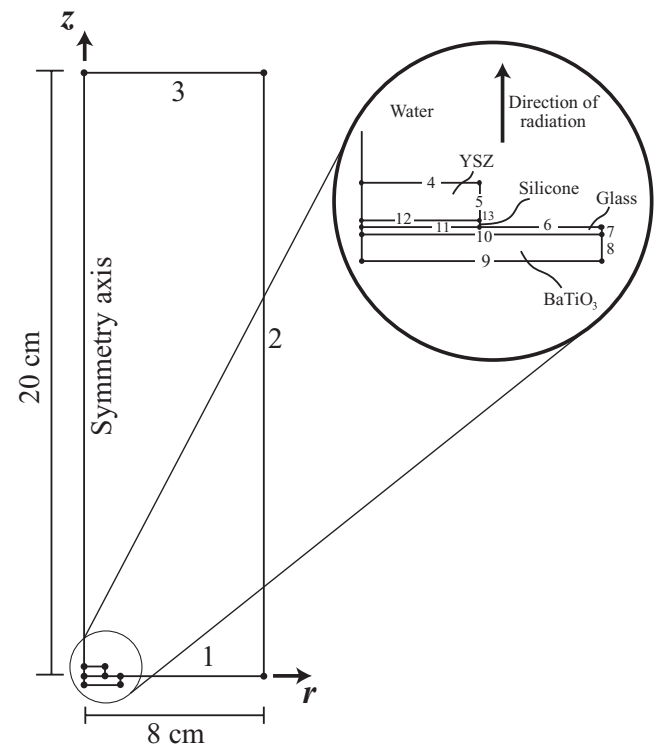


Figure 9. Geometry used for modeling the acoustic field with the FE method. Transducer was modeled as a vibrating disk of BaTiO₃ with a thin frontal protective layer of glass. The 8YSZ sample was included with a thin layer of glue.

$$\mathbf{D} = \epsilon \mathbf{E} + -\epsilon_0 \epsilon_r^S \mathbf{E} \quad (5)$$

where \mathbf{D} is the electric displacement (C m^{-2}), \mathbf{E} is the electric field (N C^{-1}), ϵ is the dimensionless strain tensor, $\boldsymbol{\sigma}$ is the stress tensor (Pa), e is the piezoelectric constant (C m^{-2}), T means the transpose, c^E is the elasticity matrix (Pa), ϵ_0 is the permittivity in vacuum ($8.854 \times 10^{-12} \text{ F m}^{-1}$), and ϵ_r^S is the relative permittivity of the material under constant strain. Nonpiezoelectric materials were solved by using Equation (4) without the term involving the electric field \mathbf{E} . Under harmonic conditions, the displacement \mathbf{u} at every point is related to the stress $\boldsymbol{\sigma}$ by the equation of motion (Newton's second law) without external volumetric forces given by

$$-\rho \omega^2 \mathbf{u} = \nabla \cdot \boldsymbol{\sigma} \quad (6)$$

By solving these equations with adequate boundary conditions at resonant frequency, the displacements of the piezoelectric disk can be obtained; the model was implemented in COMSOL Multiphysics. Boundary conditions of piezoelectric-structural simulation were configured to represent the conditions of experiments (see Figure 9). Most boundaries were set to have a free vibration condition except for the boundaries on the propagation axis; boundaries 7 and 8 were set to have only z-displacements as a piston ($\mathbf{n} \cdot \mathbf{u} = 0$), boundaries 4, 5, 6, and 13 were coupled with the acoustic pressure simulation as a structural load (\mathbf{F}_L), which depended on the normal vibration velocity ($\mathbf{v} = \nu \mathbf{n}$) and the acoustic impedance of water (Z_w) given by

$$\mathbf{F}_L = Z_w \mathbf{v} \quad (7)$$

Electric potential (20 Vp-p) and ground conditions were set on boundaries 9 and 10, respectively. The rest of the boundaries were set to have zero charge ($\mathbf{n} \cdot \mathbf{D} = 0$).

For the acoustic problem, the homogeneous Helmholtz wave equation for the harmonic radiation was used. This equation can be written as

$$\nabla^2 p + k^2 p = 0 \quad (8)$$

where k is the wavenumber ($k = \omega/c$), ω is the angular frequency in radians, and c is the speed of sound in media (which can be water, 8YSZ, glue, glass, or BaTiO₃). Boundary conditions for acoustic simulation were also set to represent the conditions during the experiments (see Figure 9). Boundaries 1, 2, and 3 were configured to match the acoustic impedance of water and reduce ultrasound reflections. Boundaries 4, 5, 6, and 13 were set with a normal acceleration dependent on the acceleration due to vibration determined with the piezoelectric-structural equations. Boundaries 8 and 9 were air-backed in the transducer so they were set in the model as sound hard boundaries ($\nu = 0$). The rest of the boundaries were configured to transmit ultrasound freely.

The piezoelectric-structural simulation was defined only for the transducer, the silicone glue (or the scalp for the second simulation), and the sample; structural and electrical properties were set at each boundary. The acoustical problem was defined for the entire geometry because the acoustic wave was present in each domain. In domains where both phenomena were present, acoustic pressure and vibration were considered linearly independent; this means that the acoustic pressure did not affect the vibration and vice versa. Both physical phenomena were connected at the boundaries radiating into the water tank as explained before. The acoustic, structural, and electric properties used for the media in the simulations are summarized in Table 1; the attenuation of glass and BaTiO₃ were included in the models according to literature.^[68,69] Although the attenuation of glue was not small, its effect in the experiments presented in this paper can be considered negligible because of its small thickness (0.1 mm); simulations not shown here with high attenuating glue did not change the results.

Postprocessing Acoustic Field: The acoustic field of ultrasound radiators is generally nonuniform since it is composed by variations of acoustic pressure around the volume. Direct comparison of measured and modeled acoustic fields would result in unreliable results; therefore,

postprocessing was carried out in order to compare both radiated fields in terms of volumetrically averaged acoustic pressure. The acoustic pressure was averaged immediately after the radiating surface to cover a cylindrical volume of 8 mm radius and 1 cm depth, with a spatial resolution of 0.7 and 1.0 mm in x- and z-directions, respectively, for the measured field, and 0.1 mm in the x- and z-directions for the modeled field. Since the 8YSZ samples did not cover entirely the transducer radiating surface, with this volume, it was possible to consider only the waves that traveled through the 8YSZ without edge waves coming from the uncovered area of the transducer. To determine the optimum volume, a simulation was made with an ideal reflector instead of 8YSZ to not have any radiation coming through the sample; this simulation helped in determining an optimum volume for postprocessing that was large enough to have sufficient data without a significant effect of radiation coming from the uncovered area of the transducer surface.

Acknowledgements

The authors would like to thank Rubén Pérez Valladares for his technical support during samples characterization. M.I.G. would like to thank UC MEXUS-CONACYT for the fellowship during the postdoctoral research at the University of California Riverside. G.A. and J.E.G. would also like to acknowledge the financial support of NSF grants 1545852 (OISE: PIRE-SOMBRERO) and 1547014 (DMR: EAGER).

Conflict of Interest

The authors declare no conflict of interest.

Keywords

biocompatible ceramics, brain therapy, cranial implants, ultrasound

Received: February 14, 2017

Revised: June 14, 2017

Published online:

- [1] J. J. Choi, M. Pernot, S. A. Small, E. E. Konofagou, *Ultrasound Med. Biol.* **2007**, *33*, 95.
- [2] F. Marquet, M. Pernot, J. F. Aubry, G. Montaldo, L. Marsac, M. Tanter, M. Fink, *Phys. Med. Biol.* **2009**, *54*, 2597.
- [3] F.-Y. Yang, W.-W. Lu, W.-T. Lin, C.-W. Chang, S.-L. Huang, *Brain Stimul.* **2015**, *8*, 465.
- [4] K. Hynynen, G. Clement, *Int. J. Hyperthermia* **2007**, *23*, 193.
- [5] Y. Tufail, A. Matyushov, N. Baldwin, M. L. Tauchmann, J. Georges, A. Yoshihiro, S. I. H. Tillery, W. J. Tyler, *Neuron* **2010**, *66*, 681.
- [6] C. Zuccato, E. Cattaneo, *Prog. Neurobiol.* **2007**, *81*, 294.
- [7] G. Leinenga, J. Gotz, *Sci. Transl. Med.* **2015**, *7*, 278.
- [8] L. Tapia-Arancibia, E. Aliaga, M. Silhol, S. Arancibia, *Brain Res. Rev.* **2008**, *59*, 201.
- [9] G. J. Siegel, N. B. Chauhan, *Brain Res. Rev.* **2000**, *33*, 199.
- [10] M. G. Murer, Q. Yan, R. Raisman-Vozari, *Prog. Neurobiol.* **2001**, *63*, 71.
- [11] A. H. Nagahara, M. H. Tuszyński, *Nat. Rev. Drug Discovery* **2011**, *10*, 209.
- [12] O. Al-Bataineh, J. Jenne, P. Huber, *Cancer Treat. Rev.* **2012**, *38*, 346.
- [13] E. Dervishi, B. Larrat, M. Pernot, C. Adam, Y. Marie, M. Fink, J. Y. Delattre, A. L. Boch, M. Tanter, J. F. Aubry, *Int. J. Hyperthermia* **2013**, *29*, 598.
- [14] H. Yu, Z. Lin, L. Xu, D. Liu, Y. Shen, *Ultrasonics* **2015**, *61*, 136.

- [15] G. ter Haar, *Prog. Biophys. Mol. Biol.* **2007**, 93, 111.
- [16] A. Burgess, Y. X. Huang, A. C. Waspe, M. Ganguly, D. E. Goertz, K. Hynynen, *PLoS One* **2012**, 7, 1.
- [17] S. Pfaffenberger, B. Devcic-Kuhar, C. Kollmann, S. P. Kastl, C. Kaun, W. S. Speidl, T. W. Weiss, S. Demyanets, R. Ullrich, H. Sochor, C. Wöber, J. Zeitlhofer, K. Huber, M. Gröschl, E. Benes, G. Maurer, J. Wojta, M. Gottsauner-Wolf, *Stroke* **2005**, 36, 124.
- [18] J. J. Choi, S. G. Wang, Y. S. Tung, B. Morrison, E. E. Konofagou, *Ultrasound Med. Biol.* **2010**, 36, 58.
- [19] A. H. Mesiwala, L. Farrell, H. J. Wenzel, D. L. Silbergeld, L. A. Crum, H. R. Winn, P. D. Mourad, *Ultrasound Med. Biol.* **2002**, 28, 389.
- [20] F. Y. Yang, G. L. Lin, S. C. Horng, T. K. Chang, S. Y. Wu, T. T. Wong, H. E. Wang, *IEEE Trans. Sonics Ultrason.* **2011**, 58, 964.
- [21] S. B. Field, N. M. Bleehen, *Cancer Treat. Rev.* **1979**, 6, 63.
- [22] S. Paliwal, S. Mitragotri, *Ultrasonics* **2008**, 48, 271.
- [23] A. Carpentier, M. Canney, A. Vignot, V. Reina, K. Beccaria, C. Horodyckid, C. Karachi, D. Leclercq, C. Lafon, J.-Y. Chapelon, L. Capelle, P. Cornu, M. Sanson, K. Hoang-Xuan, J.-Y. Delattre, A. Idbaih, *Sci. Transl. Med.* **2016**, 8, 1.
- [24] L. Pascal, G. Haïat, *Bone Quantitative Ultrasound*, Springer, NY, USA **2011**.
- [25] M. Toda, *IEEE Trans. Sonics Ultrason.* **2002**, 49, 299.
- [26] R. A. Casarotto, J. C. Adamowski, F. Falopa, F. Bacanelli, *Arch. Phys. Med. Rehab.* **2004**, 85, 162.
- [27] W. J. Elias, D. Huss, T. Voss, J. Loomba, M. Khaled, E. Zadicario, R. C. Frysinger, S. A. Sperling, S. Wylie, S. J. Monteith, J. Druzgal, B. B. Shah, M. Harrison, M. Wintermark, *N. Engl. J. Med.* **2013**, 369, 640.
- [28] B. Larrat, M. Pernot, J. F. Aubry, E. Dervishi, R. Sinkus, D. Seilhean, Y. Marie, A. L. Boch, M. Fink, M. Tanter, *Phys. Med. Biol.* **2010**, 55, 365.
- [29] N. Lynnerup, *Forensic Sci. Int.* **2001**, 117, 45.
- [30] A. Adeloje, K. R. Kattan, F. N. Silverman, *Am. J. Phys. Anthropol.* **1975**, 43, 23.
- [31] C. W. Connor, G. T. Clement, K. Hynynen, *Phys. Med. Biol.* **2002**, 47, 3925.
- [32] J. H. Song, K. Hynynen, *IEEE Trans. Bio-med. Eng.* **2010**, 57, 124.
- [33] C. R. Hill, J. C. Bamber, G. R. T. Haar, *Physical Principles of Medical Ultrasonics*, John Wiley & Sons, Chichester, UK **2004**.
- [34] K. S. Peat, R. Kirby, *J. Acoust. Soc. Am.* **2000**, 107, 1859.
- [35] K. A. Wear, *IEEE Trans. Sonics Ultrason.* **2008**, 55, 2418.
- [36] B. Emmanuel, P. Frédéric, P. Françoise, L. Pascal, *Phys. Med. Biol.* **2005**, 50, 5545.
- [37] A. B. Tamsamani, S. Vandenplas, M. L. D. Lumori, L. Van Biesen, *IEEE Trans. Sonics Ultrason.* **2001**, 48, 547.
- [38] M. Vallet-Regi, E. Ruiz-Hernandez, *Adv. Mater.* **2011**, 23, 5177.
- [39] K. Nganvongpanit, A. Phothawan, W. Pradit, S. Eitssayeam, J. Settakorn, S. Chomdej, S. Mekchay, *Chiang Mai J. Sci.* **2013**, 40, 763.
- [40] Y. Damestani, D. E. Galan-Hoffman, D. Ortiz, P. Cabrales, G. Aguilar, *Nanomedicine: Nanotechnology, Biology, and Medicine* **2016**, 12, 1757.
- [41] J. E. Alaniz, F. G. Perez-Gutierrez, G. Aguilar, J. E. Garay, *Opt. Mater.* **2009**, 32, 62.
- [42] P. Dahl, I. Kaus, Z. Zhao, M. Johnsson, M. Nygren, K. Wiik, T. Grande, M. A. Einarsrud, *Ceram. Int.* **2007**, 33, 1603.
- [43] J. Chevalier, S. Deville, E. Munch, R. Jullian, F. Lair, *Biomaterials* **2004**, 25, 5539.
- [44] J. Zhou, J. Mah, P. Shrotriya, C. Mercer, W. O. Soboyejo, *J. Mater. Sci.: Mater. Med.* **2007**, 18, 71.
- [45] G. R. Castillo-Vega, E. H. Penilla, S. Camacho-Lopez, G. Aguilar, J. E. Garay, *Opt. Mater. Express* **2012**, 2, 1416.
- [46] Y. Damestani, C. L. Reynolds, J. Szu, M. S. Hsu, Y. Kodera, D. K. Binder, B. H. Park, J. E. Garay, M. P. Rao, G. Aguilar, *Nanomedicine: Nanotechnology, Biology, and Medicine* **2013**, 9, 1135.
- [47] C. S. Desilets, J. D. Fraser, G. S. Kino, *IEEE Trans. Sonics Ultrason.* **1978**, 25, 115.
- [48] F. Zeng, S. R. Agnew, B. Raesinia, G. R. Myneni, *J. Nondestruct. Eval.* **2010**, 29, 93.
- [49] O. Balogun, R. Huber, D. Chinn, J. B. Spicer, *J. Acoust. Soc. Am.* **2009**, 125, 1437.
- [50] A. C. Dent, C. R. Bowen, R. Stevens, M. G. Cain, M. Stewart, *J. Eur. Ceram. Soc.* **2007**, 27, 3739.
- [51] D. Berlincourt, H. H. A. Krueger, C. Near, Properties of Piezoelectricity Ceramics, Morgan Electro Ceramics, Wrexham, UK **1999**.
- [52] G. D. Ludwig, *J. Acoust. Soc. Am.* **1950**, 22, 862.
- [53] D. M. Nell, M. R. Myers, *J. Acoust. Soc. Am.* **2010**, 127, 549.
- [54] M. Martins, V. Correia, J. M. Cabral, S. Lanceros-Mendez, J. G. Rocha, *Sens. Actuators, A* **2012**, 184, 141.
- [55] F. J. Fry, J. E. Barger, *J. Acoust. Soc. Am.* **1978**, 63, 1576.
- [56] H. Hori, G. Moretti, A. Rebora, F. Crovato, *J. Invest. Dermatol.* **1972**, 58, 396.
- [57] M. I. Gutierrez, H. Calas, A. Ramos, A. Vera, L. Leija, *Ultrasonics* **2012**, 52, 767.
- [58] M. Willatzen, *IEEE Trans. Sonics Ultrason.* **2001**, 48, 100.
- [59] J. L. San Emeterio, A. Ramos, P. T. Sanz, A. Ruiz, *Ferroelectrics* **2002**, 273, 2675.
- [60] E. H. Penilla, C. L. Hardin, Y. Kodera, S. A. Basun, D. R. Evans, J. E. Garay, *J. Appl. Phys.* **2016**, 119, 1.
- [61] E. H. Penilla, Y. Kodera, J. E. Garay, *Adv. Funct. Mater.* **2013**, 23, 6036.
- [62] A. Ramos, J. L. San Emeterio, P. T. Sanz, *Ultrasonics* **2000**, 38, 553.
- [63] R. B. Houghton, D. C. Obray, (Mettler Electronics Corp.), US 5095890, **1992**.
- [64] E. P. Papadakis, *J. Acoust. Soc. Am.* **1968**, 44, 724.
- [65] D. Boucher, M. Lagier, C. Maerfeld, *IEEE Trans. Sonics Ultrason.* **1981**, 28, 318.
- [66] Y. Kagawa, T. Yamabuchi, *IEEE Trans. Sonics Ultrason.* **1976**, 23, 379.
- [67] H. A. Kunkel, S. Locke, B. Pikeroen, *IEEE Trans. Sonics Ultrason.* **1990**, 37, 316.
- [68] U. C. Naithani, D. S. Lingwal, A. Kumar, S. C. Deorani, B. S. Semwal, *Sri Lankan J. Phys.* **2000**, 1, 81.
- [69] M. Leonard, *Handbook of Reference Data for Nondestructive Testing*, ASTM International, Baltimore, MD, USA **2002**.
- [70] J. Lubbers, R. Graaff, *Ultrasound Med. Biol.* **1998**, 24, 1065.
- [71] Saint-gobain, Physical Properties of Glass, <http://uk.saint-gobain-glass.com/trade-customers/physical-properties> (accessed: February 2016).
- [72] Azo Materials, Properties: silicone rubber, <http://www.azom.com/properties.aspx?ArticleID=920> (accessed: February 2016).
- [73] S. A. Goss, R. L. Johnston, F. Dunn, *J. Acoust. Soc. Am.* **1978**, 64, 423.
- [74] X. Liang, S. A. Boppart, *IEEE Trans. Biomed. Eng.* **2010**, 57, 953.
- [75] R. Grahame, P. J. Holt, *Gerontologia* **1969**, 15, 121.
- [76] J. Y. Rho, R. B. Ashman, C. H. Turner, *J. Biomech.* **1993**, 26, 111.
- [77] R. Shahar, P. Zaslansky, M. Barak, A. A. Friesem, J. D. Currey, S. Weiner, *J. Biomech.* **2007**, 40, 252.